

OMAE2022-79718

HYDRODYNAMIC COEFFICIENTS OF GENERIC SUBSEA MODULES IN FORCED OSCILLATION TESTS – IMPORTANCE OF STRUCTURE PARTS

Mia Abrahamsen-Prsic
SINTEF Ocean
Trondheim, Norway

Frøydis Solaas
SINTEF Ocean
Trondheim, Norway

Trygve Kristiansen
Norwegian University of
Science and Technology
Trondheim, Norway

ABSTRACT

A systematic study of the hydrodynamic coefficients for simplified subsea modules has been performed, to support the estimation of the coefficients needed for planning of subsea installation operations. The coefficients are assessed for a nearly two-dimensional test setup. The tests are performed as forced oscillations at various amplitudes and periods, representing the forces on the module lowered through the water column.

The importance of each of the main components of the subsea modules – mudmat, protection roof and process equipment of different shapes inside the modules are studied at fully submerged condition. Results for the module elements, generic contents and different combinations of these elements are presented.

For the tested modules, damping is generally the dominating hydrodynamic force. However, the presence of the content inside the modules will generally increase the importance of added mass.

Estimation of the hydrodynamic coefficients by summation of the coefficients for the individual structure elements generally overestimates the damping, compared to the coefficients measured for the complete modules. For added mass, estimation based on summation gives generally good results.

Keywords: Hydrodynamic coefficients; Marine Operations; Subsea modules; Added mass and damping.

NOMENCLATURE

A = hydrodynamic added mass in vertical direction (kg)
A₀ = infinite fluid hydrodynamic added mass for a two-dimensional solid plate, as predicted by potential flow theory (kg)
B = damping in vertical direction (kg/s)
D = total width of model (m)
F_z = net force on the model (N)
f = sampling frequency in the experimental campaign (1/s)
H = height of the model (m)

L = length of model (m); L=0.57 m in all experiments
M = dry mass of the model (kg)
n = number of forces oscillations used for data analysis
n_{tot} = number of sampling points within the time series
T = period of forced oscillation (s)
U = velocity amplitude (m/s)
Z = amplitude of oscillatory motion
 \ddot{z} = acceleration in vertical direction (m/s²)
 \dot{z} = velocity in vertical direction (m/s)
 τ = perforation ratio (open area/total area)
 ρ = water density (kg/m³); $\rho=1000$ kg/m³ in all tests
 ω = frequency of oscillation (rad/s)

1. INTRODUCTION

Preparing for the installation of a subsea module, necessary vessel- and crane capacity, as well as the limiting sea-state for the operation need to be determined. Numerical modelling and simulations are commonly used to assess the forces in the lifting equipment and on the module. The predictions are in many cases depending on the hydrodynamic coefficients used for the structure of interest.

The coefficients for a subsea module can be estimated through model tests, numerical / CFD simulations of the entire structure or estimations based on experience. In most cases, both physical and numerical modelling are demanding and costly. The coefficients are therefore often estimated manually, based on published data for similar structures and/or idealized structure elements. Rough estimates can lead to uncertainties - overestimation of expected loads unnecessarily narrows the weather window or leads to overcompensation of vessel prerequisites. Underestimated loads potentially endanger the personnel and equipment during a high-risk operation.

The motivation for this work is thus to reduce the uncertainty when performing marine deployment operations, which is likely to reduce the conservatism and delays in increasingly more demanding operations and harsher

environments. The objective is to increase the knowledge of the hydrodynamic loads on typical members of subsea structures, and combinations of the main components, to account for interaction effects between different member types.

A generalized subsea module is divided in main components – a mudmat, a protection roof and process equipment. A mudmat, often consisting of several side-by-side plates with low perforation ratio, is here represented by four parallel solid plates. The protection roof, commonly consisting of grillage and protective cage, is modelled by a perforated plate. Several generic models, consisting of square cylinders, are used for the process equipment. Detailed description of the elements and generalized subsea modules is presented in Section 2.1.

Hydrodynamic behavior of simple structures - circular cylinders and slender bodies has been described in detail in several textbooks, such as Sumer and Fredsøe [1] and Zdravkovich [2]. Recommended practice for modelling and analysis of marine operations provides simplified formulations for establishing design loads [3]. As perforated plates appear in various marine applications, both analytical, numerical and experimental investigations have been published. Molin presented an extensive review in 2011 [4]. Other relevant studies include, amongst others, An and Faltinsen [5] and Tian et al. [6]. Sarkar and Gudmestad [7] have discussed the challenges with estimating the effects of perforation when using the DNVGL-RP-N103 [3]. In the present project, perforated plates have been analyzed experimentally and numerically, published by Mentzoni et al. [8] - [10]. Several configurations of side-by-side plates – tandem and four-plate configurations, mimicking the subsea modules' mudmats, have been discussed by Solaas et al. [11]. Another initial study of the present project, [12] presents experimentally obtained added mass and damping coefficients for different configurations of perforated plates and cylinders.

This paper is focusing on estimation of added mass and damping coefficients, obtained and calculated as described in Section 2. The hydrodynamic coefficients are measured for separate main components of the subsea modules (mudmat, protection roof and process equipment), as well as combinations and generic modules with varying equipment contents – as shown Section 3. The results are presented in Section 4, where amplitude and period dependency are discussed, as well as interaction effects and dominating hydrodynamic factors.

2. METHODOLOGY AND SETUP

2.1. Experimental method

The experimental campaign is conducted in one of the wave flumes at the Marine Technology Center in Trondheim, Norway. The flume is a 13.5m long glass tank with 0.60m width and 1.4m depth. The flume is equipped with parabolic beaches at both ends of the tank, minimizing the radiated waves' reflections. The model is placed in the middle of the tank, 6.5m from the apex of each beach. The water depth is 1.0m for all tests. A schematic representation of the setup is presented in FIGURE 1.

The models are tested in forced oscillations. To avoid the end-effects, near two-dimensionality is accomplished by

mounting the models between two rigid, vertical acrylic plates. The plates are fixed on a steel frame, attached rigidly to an actuator, and oscillate parallel to the walls of the glass flume tank, with a gap of 9mm between the oscillating plates and the tank walls. The bottom edge of the acrylic plates. The bottom edge is furthermore shaped as a sharp wedge, to minimize the hydrodynamic impact. The distance between the plates determines the length of the models, $L = 0.57\text{m}$ for this entire study. The actuator oscillates in the vertical direction along a rail-supported threaded drive shaft, connected to an electrical motor through a belt drive. The actuator is driven by a prescribed sinusoidal forced oscillation, read at the sample frequency of 50Hz.

The force on the entire rig, including the frame, acrylic plates, and the model, is measured by a 2DOF force transducer located in the intersection between the model rig and the actuator. Six 3DOF accelerometers, mounted at the rig and the acrylic plates, are registering the position. The wave surface elevation is monitored by 6 wave probes, positioned at three distances between the rig and the beaches. All measurements are recorded at a sample rate of $f = 200\text{Hz}$, with Butterworth filtering at 20Hz. The measurements are also band-pass filtered around the basic harmonic of the oscillation.

The test sequences consist of harmonically varying signals, with a given amplitude and period of oscillation. Each sequence consists of 20 periods of oscillations. The first five and the last five are used to ramp the signal gradually from/to zero to/from the prescribed amplitude of motion. [12] provides more details about the test setup and the measurements, as well as a discussion about the accuracy of the experiments.

2.2. Data analysis – hydrodynamic coefficients

The experimental results are presented in terms of hydrodynamic coefficients, and will be discussed through dependency on the Keulegan–Carpenter number, KC , and the oscillation period, T . The added mass and damping coefficients are calculated based on the measured acceleration and the forces on the entire rig. To determine the force on the model only, the time sequences have been run for the empty rig (the frame and the acrylic plates only). The measured force is subsequently subtracted from the total force, time-step by time-step, resulting in net force exerted on the model.

For each of the amplitudes and periods tested, added mass and damping are extracted based on the following standard formulation:

$$F_z = (M + A)\ddot{z} + B\dot{z} \quad (1)$$

where M is the dry mass of the model, A the added mass, \ddot{z} the acceleration, B the damping, \dot{z} the velocity, and F_z the measured net force. Since the model is oscillating harmonically, the added mass and damping are obtained by Fourier averaging:

$$(M + A) \int_T \ddot{z} \, dt + 0 = \int_T F_z \, dt \quad (2)$$

$$0 + B \int_T \dot{z} \, dt = \int_T F_z \, dt \quad (3)$$

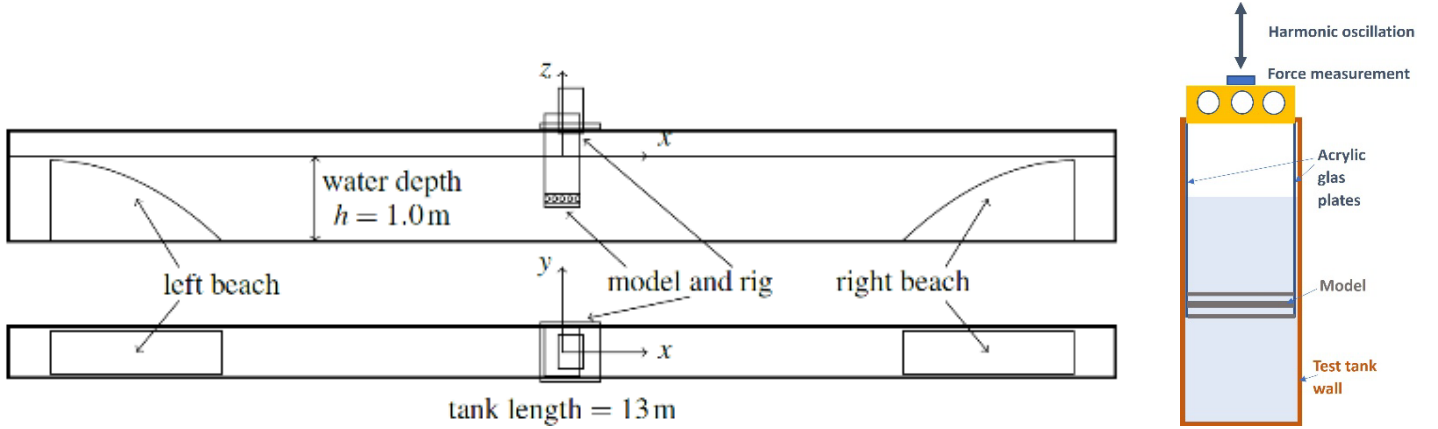


FIGURE 1: Experimental configuration - the tank with the model and oscillating rig. Side view (up), top view (bottom), vertical cross-section (right). Figure taken from [12].

The integrations are performed over entire periods of oscillations, T , and integration is performed over $n = 8$ of the ten steady-state forcing periods, avoiding the first and last forcing periods as well as the ten periods of the ramp-in and -out.

Number of sampling points within the used time series is thus $n_{tot} = n T/f$. All quantities are band-pass filtered around the basic forcing harmonic, removing the noise in the measurements as well as the higher harmonics in the hydrodynamic forcing. An example is presented in FIGURE 2.

The presented results are based on the mean of the coefficients for eight analyzed oscillations. Standard deviation is presented as error bars in several figures in Section 4, demonstrating the variations between these 8 individual cycles within each test.

The force coefficients are presented as function of the Keulegan-Carpenter number:

$$KC = \frac{UT}{D} \quad (4)$$

which relates the vertical velocity magnitude, U , to the period of oscillations, T , and the characteristic model length, D . For harmonic motions, the KC number simplifies to

$$KC = 2\pi \frac{Z}{D} \quad (5)$$

with Z being the amplitude of the harmonic motion.

The tested amplitudes of vertical forced motion range from 16mm to 166mm, corresponding to KC numbers from 0.25 to 2.5 for a characteristic length $D = 0.42\text{m}$, which is the width of the tested simplified subsea modules. For a full-scale module with a characteristic length of 10m, the range of KC numbers corresponds to wave amplitudes from 0.4m to 4.0m, and the tested periods of oscillation, $1.0\text{ s} \leq T \leq 2.0\text{ s}$, correspond to full-scale wave periods from 4.9 s to 9.8 s.

The data presentation is generally based on the dimensionless hydrodynamic coefficients. The added mass coefficients are made non-dimensional by the infinite fluid added mass for a two-dimensional solid flat plate, predicted by potential flow theory:

$$A_0 = \rho \pi \frac{D^2}{4} L \quad (6)$$

Here, $D = 0.42\text{m}$, $L = 0.57\text{m}$.

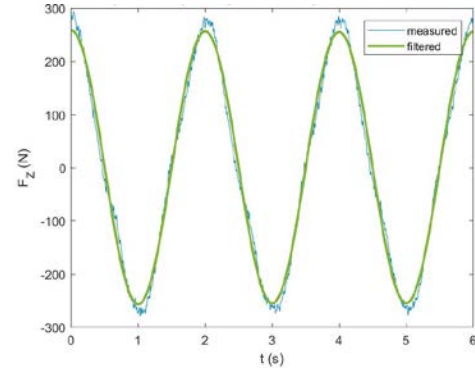


FIGURE 2: An example of the measured and the band-pass filtered time-series of the force measurements.

For the single square cylinder (1SQ) tested alone, A_0 is calculated as the added mass for a two-dimensional rectangle with width to height ratio of 1.0, given in DNVGL-RP-N103 [3]:

$$A_0 = 1.51 \rho \pi \frac{D^2}{4} L \quad (7)$$

where, $D = 0.06\text{ m}$ and $L = 0.57\text{ m}$.

To provide the dimensionless damping coefficients, normalization with the solid plate added mass, A_0 , multiplied by the circular frequency, ω , is used. Since the structures are oscillating harmonically, the ratio between the damping force F_d and the inertia force F_i is:

$$\frac{F_d}{F_i} = \frac{B \frac{2\pi Z}{T}}{A \left(\frac{2\pi}{T}\right)^2 Z} = \frac{1}{2\pi} \frac{BT}{A} = \frac{B}{A\omega} \quad (8)$$

Therefore, if the relation $B/(A\omega)$ is larger than 1, the damping force is the dominating hydrodynamic force. For values smaller than 1, the added mass is dominating.

2.3. Validation - repeatability

To check the repeatability of the measurements, forced oscillations of the subsea module PP+4P43B+35SQ (see TABLE 2) are performed three times in course of the experimental campaign. Consistency of the results is presented in FIGURE 3, through the averaged net force maxima, exerted on the module. For each examined period of oscillations, the three tests are in

good agreement, as the largest discrepancy between the measurements remains within 2.5%.

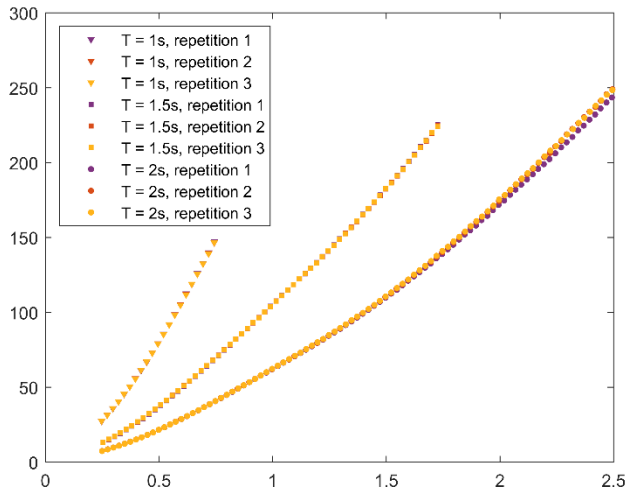


FIGURE 3: Repetition tests for the model PP+4P43B+35SQ. Net measured force. $H = 0.12\text{m}$.

It is seen from FIGURE 3 that repetition 1 deviates slightly from the other two runs. The reason for this may be the variations

TABLE 1: Main particulars of the structure elements

		<p>Perforated plate: PP Perforation ratio $\tau = 0.28$ Main dimension $D = 0.42\text{ m}$ Model mass = 2.132 kg $A_0 = 79.0\text{ kg}$</p>
		<p>Mudmat model 4P43B: Perforation ratio $\tau = 0.43$ Main dimension $D = 0.42\text{ m}$ Gap: 2 x 9 cm Model mass = 1.891 kg $A_0 = 79.0\text{ kg}$</p>
		<p>Content: Square 1SQ Rectangular cylinder: 6 cm x 6 cm Main dimension: $D = 0.06\text{ m}$ Model mass = 1.58 kg $A_0 = 2.43\text{ kg}$</p>
		<p>Content: Grid 35SQ 7 x 5 = 35 rectangular 1 cm x 1 cm staggered cylinders. Main dimension $D = 0.42\text{ m}$ Model mass = 2.734 kg $A_0 = 79.0\text{ kg}$</p>
		<p>Content: 5SQ 5 rectangular 6 cm x 6 cm cylinders. Main dimension $D = 0.42\text{ m}$ Gap: 4 x 3 cm Model mass = 7.68 kg $A_0 = 79.0\text{ kg}$</p>

in temperature. The water was kept at quite stable temperature, 22.4°C at repetition 1, and 23.1°C for the other two. The force gauge was, however, air-mounted, thus exposed to larger day-night variations in the ambient temperature. Repeatability of the measurements with this experimental setup is also discussed in [10] and [12].

2.4. Scaling of the model test results

The presented data may be scaled to full scale dimensions by use of the scaling factors given below. The scaling factor $\lambda = D_{\text{STRUCTURE}}/D_{\text{MODEL}}$, where D is the main dimension of the structure. With a main dimension of the module models equal to 0.42 m, the scaling factor in the tests may be from around 20 to 40, dependent on the structure in question. The tests were performed in fresh water with a density of approximately 1000 kg/m³. If the density of the sea water is 1025 kg/m³, a factor of 1.025 comes to addition to the quantities containing mass (kg).

3. MODEL CONFIGURATIONS

The tested models consist of various combinations of generalized structure elements. The elements, in stand-alone tests, are shown in TABLE 1.

The protection structure roof is modelled as a perforated steel plate with 28% perforation ratio (PP), which is within the perforation ratio span of the hatch covers used on commercial subsea modules. The length of the plate is 0.57 m, width 0.42 m, and the thickness 4mm, ensuring a rigid model that does not bend or vibrate in course of the test runs.

The mudmat model consists of four side by side solid steel plates separated by two slots (4P43B). Solid plates are chosen in accordance with DNVGL [3], stating that plates with perforation ratio less than 5% (as common in standard mudmats) may be regarded as solid. Each of the plates has a length of 0.57 m, width 0.06m and plate thickness 4 mm. The width of the two slots between the plates is 0.09m and the total width of the mudmat is equal to the width of the perforated plate, 0.42 m.

Three simplified, generic versions of the subsea equipment inside the modules are tested. The first representation consists of a single 60 mm x 60 mm square cylinder (1SQ). The element is filled with firm foam to prevent water from seeping into the model. The second version consists of a staggered grid of 7 x 5 rectangular cylinders, each with 10 x 10 mm cross-section (35SQ). The total volume of the grid is nearly equal to the volume of the single square, 3500 mm² and 3600 mm², respectively. The third version consists of a row of five 60 mm x 60 mm square cylinders (5SQ).

Simplified subsea modules are modelled as combinations of these elements. Most of the setups represent the whole simplified subsea modules, and consist of the protection roof, the mudmat and one of the generic contents. The models are mounted with different distances between the roof and the mudmat, 0.12m and 0.18m. Thus, the height to width ratio, H/D is 0.29 and 0.43, targeting commercial subsea modules.

Series of tests are performed for a simplified model without any contents, consisting of the perforated plate and the mudmat (PP&4P43B). Combinations of only mudmat and the contents, as well as protection roof and the contents are also tested. An overview of the models studied in this report is given in TABLE 2, with name, abbreviation, model height, mass and reference added mass (A_0).

4. RESULTS AND DISCUSSION

The experiments are performed for each main components of a simplified subsea module, as an isolated body, and the complexity is further increased by combining the elements and varying the contents of the modules. Perforated plates, representing the protective roof of a generic subsea module, have been extensively discussed in several previous publications [8] - [10], including both the experimental results with the same setup as present, as well as simplified numerical solutions and CFD. Hydrodynamic behavior of mudmats has been explored in [11] and [14]. Here, the hydrodynamic coefficients were presented systematically for a single thin plate, two plates in tandem, and for four plates in several configurations corresponding to the shapes of the subsea modules' mudmats. The results are again discussed through experimental and CFD simulations, and the repeatability and quality of the results is assessed. These

components will therefore not be discussed in detail in this paper, and only a short overview is presented in Section 4.1. The main focus is on the analysis of the models assembled of several main components – protection roof and mudmat, with or without any generic contents. The results are presented in Section 4.2, through KC and T dependency, as well as by assessment of the coefficients by summation of individual elements versus the measured coefficients for entire modules.

4.1. Individual main components

Hydrodynamic coefficients for the perforated plate (PP) and the mudmat (4P43B) are presented in FIGURE 4 to FIGURE 6. FIGURE 4 shows that the added mass of the mudmat is dependent on the amplitude of oscillation (KC number) and is increasing monotonically for the considered span of KC. Added mass is dependent on the configuration of the mudmat, though. [11] tested a mudmat with the same perforation ratio as here, but with a different distribution of the plates. The four plates were distributed uniformly, with the same gap between each pair. For the same KC range, that configuration yields A/A_0 about 30 - 50% lower than the present mudmat. The trend of near-linear increase across KC span is, however, similar for different mudmat shapes, including the cases with only two side-by-side plates [11]. Added mass of the perforated plate, on the other hand, shifts the slope at $KC \approx 1.2$ (FIGURE 4). This is contributed to the presence of the end vortices, which become a dominant part of the force for larger KC [15]. The perforation ratio of the present perforated plate is 0.28. In [9], results for plates with different τ are presented. Added mass is highly dependent on the porosity ratio of the plate, but the trend of the curve is the same for all τ in range between 0 and 0.5.

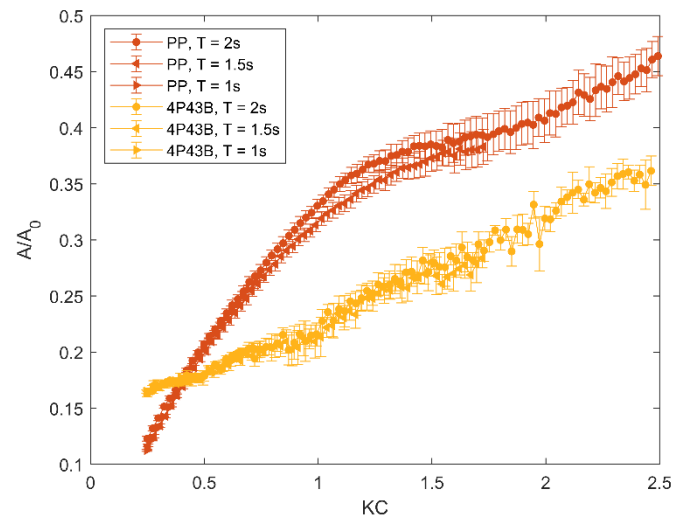
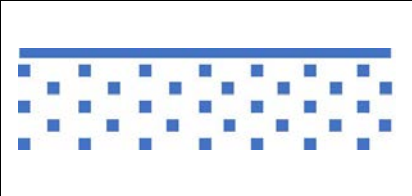
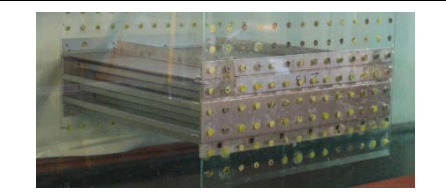
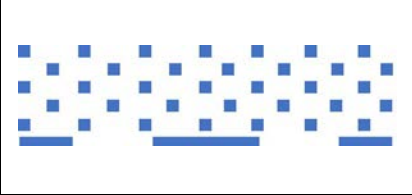
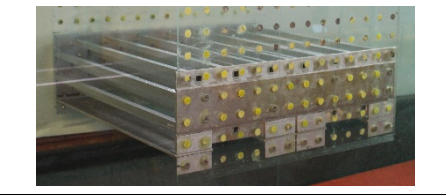

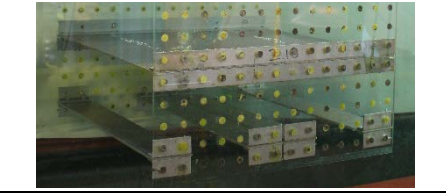
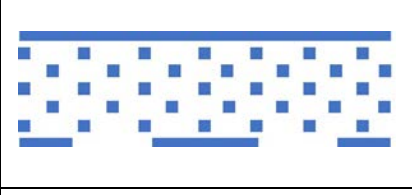

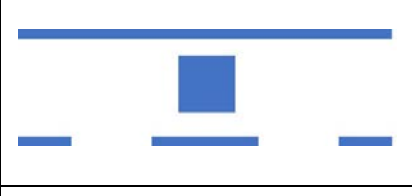
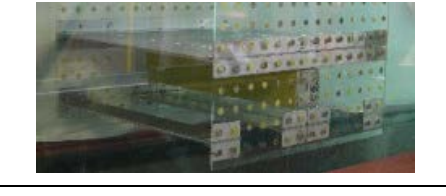
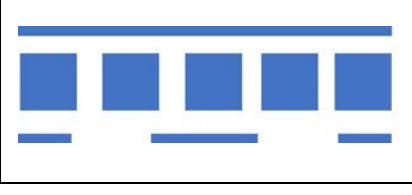
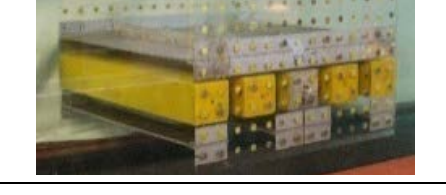


FIGURE 4 Normalized added mass of the protection roof, $\tau = 0.28$ (red) and mudmat, $\tau = 0.43$ (yellow), at three periods of oscillation ($T = 2s, 1.5s, 1s$). Standard deviation is presented as error-bars.

TABLE 2: Overview over studied configurations for simplified subsea modules, containing combinations of protection roof, mudmat and various generic process equipment.

		<p>Module: PP&35SQ Perforated plate, $\tau = 0.28$ Content: Grid 35SQ H = 0.12m Model mass = 4.866 kg</p>
		<p>Module: 4P43B&35SQ Mudmat, $\tau = 0.43$ Content: Grid 35SQ H = 0.12m Model mass = 4.598 kg</p>
		<p>Module: PP&4P43B Perforated plate, $\tau = 0.28$ Mudmat, $\tau = 0.43$ H = 0.12m, 0.18m Model mass = 3.995 kg</p>
		<p>Module: PP&4P43B&35SQ Perforated plate, $\tau = 0.28$ Mudmat, $\tau = 0.43$ Content: Grid 35SQ H = 0.12m, 0.18m Model mass = 6.73 kg</p>
		<p>Module: PP&4P43B&1SQ Perforated plate, $\tau = 0.28$ Mudmat, $\tau = 0.43$ Content: Square 1SQ H = 0.12m, 0.18m Model mass = 5.603 kg</p>
		<p>Module: PP&4P43B&5SQ Perforated plate, $\tau = 0.28$ Mudmat, $\tau = 0.43$ Content: Five squares 5SQ H = 0.12m Model mass = 11.678 kg</p>

The damping of both PP and 4P43B is increasing significantly with increasing amplitude, as shown in FIGURE 5. The damping is also depending on the arrangement of the plates in the mudmat, but the difference between the configurations tested in [11] is smaller, 10 – 20%. An increase in perforation ratio of the protection roof results in a decrease of the damping coefficients at any tested KC, and in a milder gradient of the $B/\omega A_0$ curve [9].

Damping to added mass ratio is shown in FIGURE 6. Both PP and 4P43B have a damping to added mass relation larger than 1, which means that the hydrodynamic forces are dominated by the damping. The dominance of the damping is more significant for the perforated plate than for the mudmat. The difference is especially prominent for lowest tested KC.

Results for the three different models of the generic process equipment (1SQ, 5SQ and 35SQ) are presented in FIGURE 7 and FIGURE 8. The results are presented by means of amplitude of forced oscillations. KC is not directly comparable due to the large difference in the models' normalization width ($D_{1SQ} = 0.06m$ while all other models have $D = 0.42m$). On the other hand, volume of the models 1SQ and 35SQ is nearly the same.

The damping to added mass relation is shown in FIGURE 7. Except for the largest amplitudes, added mass is dominating the hydrodynamic force for 1SQ. The damping is dominant for $KC > 14$ - KC number normalized by the width of the other models equals to 2.0. The damping to added mass ratio curve for 35SQ has a much sharper inclination and the damping

is the dominant force for $KC > 0.44$ (amplitudes larger than 0.03m). Observing the dimensional net force, it is seen from FIGURE 8, that the forces for the single square are smaller than for the staggered grid, despite comparable displacement of the models. This may be explained by interaction effects between the squares and end vortices, similar as for the perforated plates.

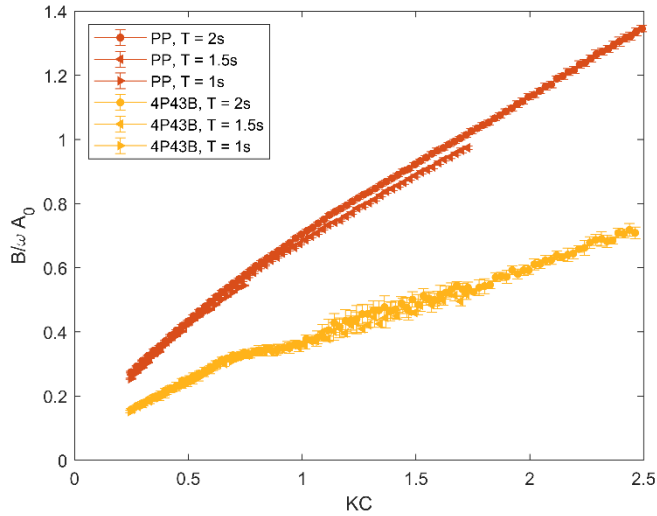


FIGURE 5 Normalized damping of the protection roof tested alone (red) and mudmat tested alone (yellow), at three periods of oscillation ($T = 2s, 1.5s, 1s$). Standard deviation is presented as error-bars.

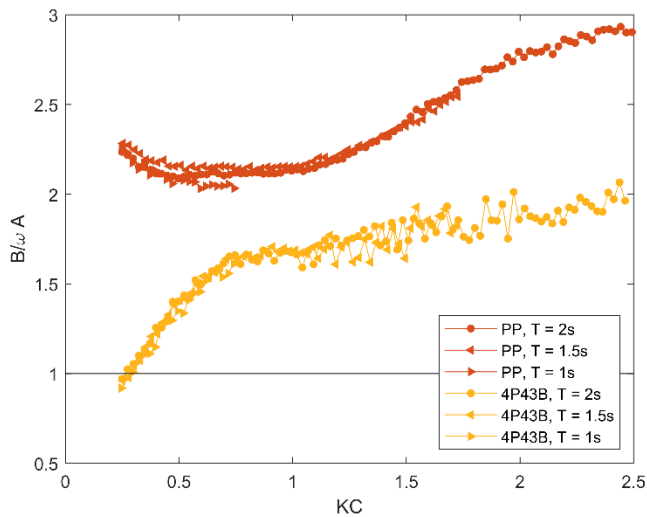


FIGURE 6 Damping to added mass ratio of the protection roof tested alone (red) and mudmat tested alone (yellow), at three periods of oscillation ($T = 2s, 1.5s, 1s$).

Net forces exerted on the third generic content, 5SQ, are significantly higher than for 1SQ and 35SQ, as expected due to 5 times larger displacement (FIGURE 8). The measured forces on 5SQ are also compared to the coefficients obtained by multiplying the results for 1SQ by 5. It is clearly seen that $5 \times 1SQ \neq 5SQ$. The force for 5SQ, calculated by summation of the force for 5 single squares is significantly underestimated. This indicates that the interaction effects between the squares in the

configuration are crucial for the hydrodynamic forcing. This indicates that 5SQ acts more as a perforated plate/screen, for which hydrodynamic interaction is important, see also [14].

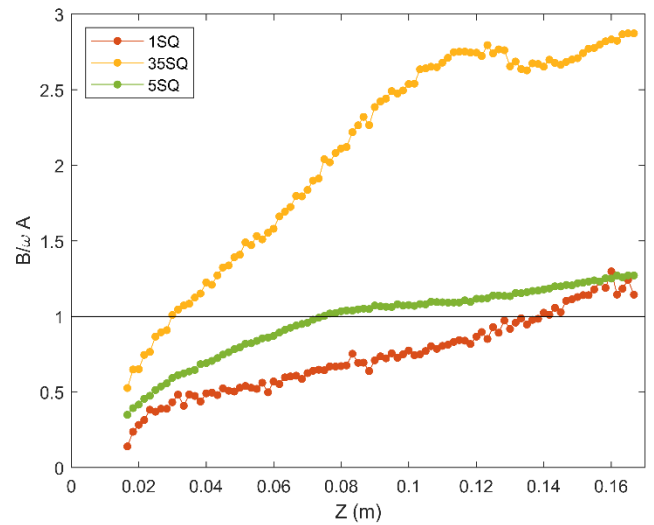


FIGURE 7 Damping to added mass ratio for generic process equipment (1SQ, 35SQ, 5SQ), tested alone. $T = 2s$.

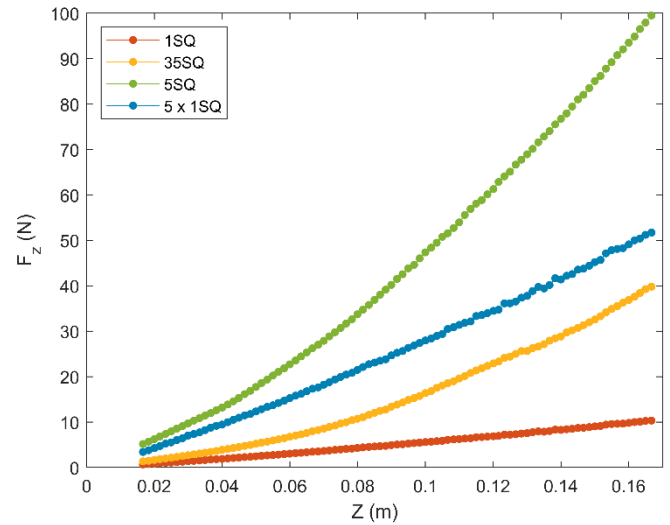


FIGURE 8 Net force for generic process equipment (1SQ, 35SQ, 5SQ, 5 x 1SQ), tested alone. $T = 2s$.

The damping to added mass relation shows that the contribution from the damping is generally larger for 5SQ than for 1SQ. An interesting observation, however, is that the damping to added mass relation is quite similar for these two models, at the smallest and the largest amplitudes of motion.

4.2. Simplified subsea modules

The following Section is assessing the simplified subsea modules modelled as combinations of a perforated plate, mudmat and generic contents (TABLE 2). One can see that removing of either the mudmat (PP&35SQ) or the protection roof (4P43B&35SQ) results in comparable reduction in added

mass (FIGURE 9a). Removing the contents leads to smaller difference in A/A_0 , compared to the entire module. FIGURE 9b displays only a minor difference in $B/\omega A_0$ ratio between the module with and without any contents. The discrepancy for the module without the mudmat are somewhat larger, while the smallest damping is obtained for the module without the perforated plate.

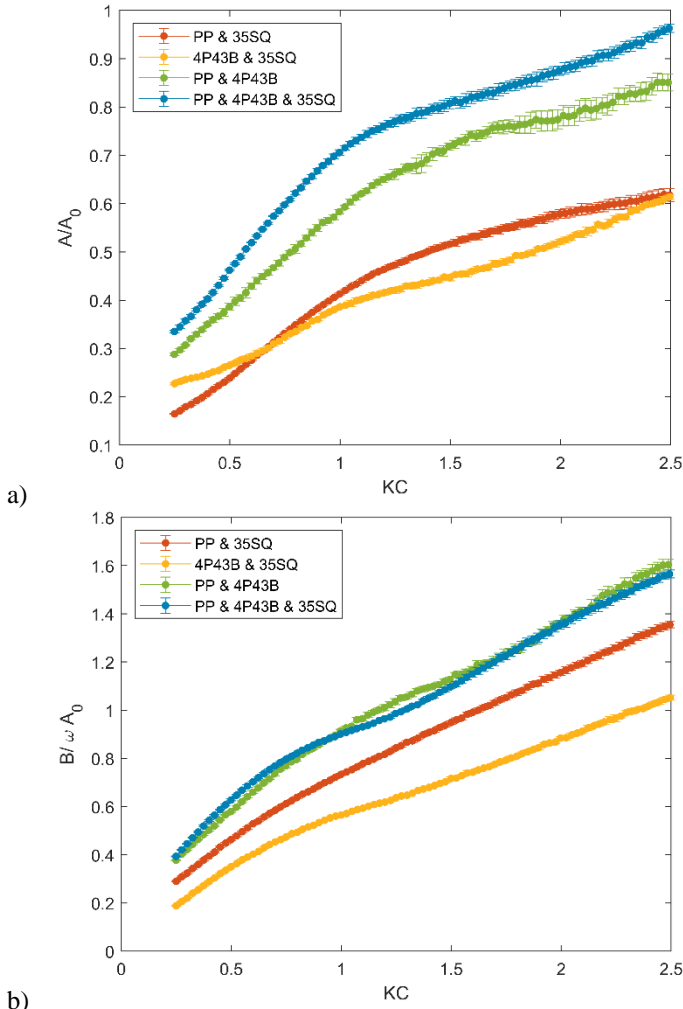


FIGURE 9 Added mass and damping for a subsea module consisting of: roof and contents; mudmat and contents; roof and mudmat; roof, mudmat and contents. $H = 0.12\text{m}$; $T = 2\text{s}$.

The influence of the presence of the contents within the subsea module is presented in FIGURE 10 and FIGURE 11. The results are compared for the models with height $H = 0.12\text{m}$ and $H = 0.18\text{m}$. For the present nearly two-dimensional test set-up, there are only small differences between the coefficients for the two heights.

The largest added mass is obtained for the module with the five large squares, somewhat lower for the modules with the staggered grid inside. Added mass for the module without any content and the module with one single large square inside is nearly the same, with closest results for small KC numbers.

Damping, as a function of KC number, is compared in FIGURE 11. For the smallest KC numbers, the damping for the modules with and without any content is equal. As KC increases, the damping for the module with the five large squares is increasing slower than for the other contents. The other three are increasing at comparable rate.

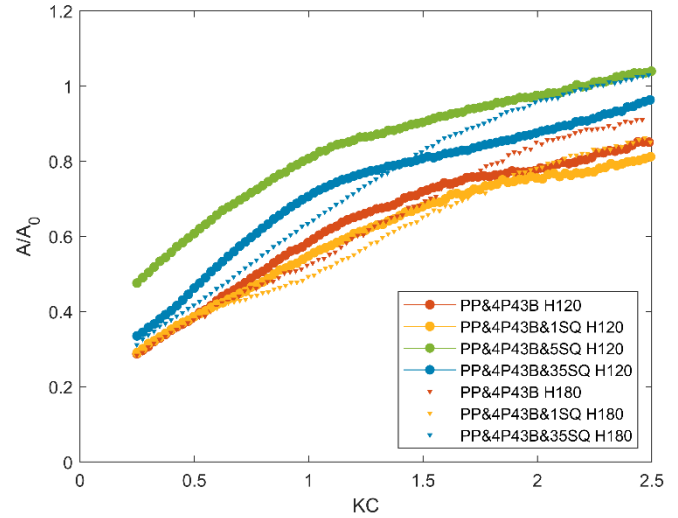


FIGURE 10 Added mass for a subsea module without any contents, with 1SQ, 5SQ and 35SQ. Model height $H = 0.12\text{m}$ (circles) and $H = 0.18\text{m}$ (dots); $T = 2\text{s}$.

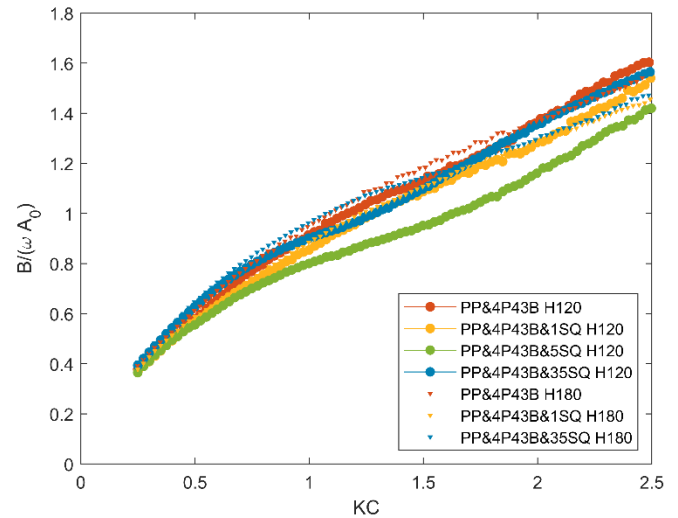


FIGURE 11 Damping for a subsea module without any contents, with 1SQ, 5SQ and 35SQ. Model height $H = 0.12\text{m}$ (circles) and $H = 0.18\text{m}$ (dots); $T = 2\text{s}$.

The dependency of the hydrodynamic coefficients on the period of forced oscillations is shown in FIGURE 12. Damping of the module PP&4P43B, with $H = 0.18\text{m}$ is used as an example, at periods of 2, 1.75, 1.5, 1.25 and 1 s. Shorter periods of oscillations lead to a decrease in the damping, with larger differences at higher KC. Here, one should consider the relatively large amplitude of the forced oscillations, up to 0.167m, compared to only 0.41m of water column above and

below the protection roof and the mudmat. Wave radiation damping is thus calculated according to Faltinsen [13] and presented as thin solid lines in FIGURE 12. The contribution of the wave radiation is in the same range as the difference between the damping for various periods at given KC and explains the majority of the discrepancies. Period dependency is thus considered to be negligible.

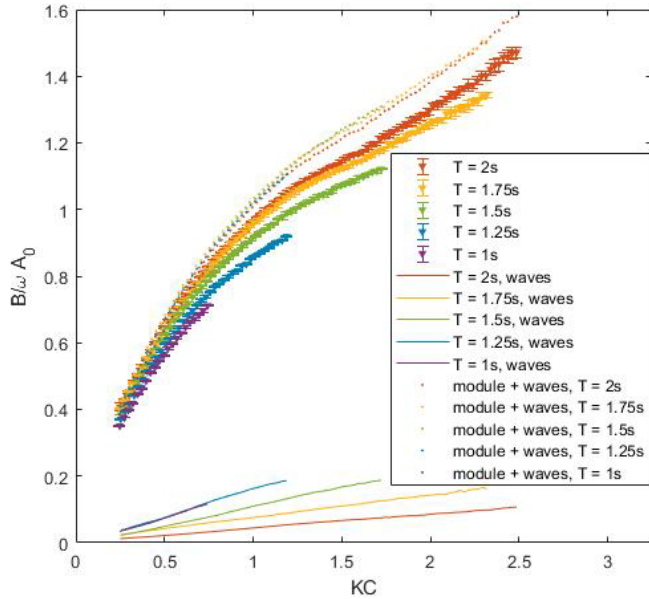


FIGURE 12 Damping for the simplified subsea module without any contents (PP&4P43B), $H = 0.18\text{m}$, at various periods of forced oscillations. Estimated wave radiation damping for respective periods – solid lines. Damping for the module + wave radiation damping – dotted line. Standard deviation is presented as error-bars.

4.3. Comparison with numerical simulations

The hydrodynamic coefficients for one of the tested configurations, PP&4P43B, are calculated by an in-house CFD code [15], also used for modelling of mudmats [11], plates of various porosities [9] and two parallel perforated plates [15]. A two-dimensional, laminar Navier-Stokes solver is applied, using Cartesian, staggered grid, with variable mesh size across the domain. Period of oscillation is $T = 2\text{s}$, and the density and the kinematic viscosity are chosen to correspond to the ones in the experimental campaign. Detailed description of the numerical model, as well as validation and verification study on the example of perforated plates, are published in [8]. The same CFD code is used for the modeling of the mudmat used in the present study (4P43B), published in [11]. The method performs reliably for the subsea modules' main components - perforated plates [8] and mudmats. [11] presented a parametric study of simplified mudmats, consisting of two or more solid side-by-side plates, at various distances, while [8] presents results for the hatch cover type components with different perforation ratios.

For a simplified module, consisting of a mudmat and protection roof, CFD results are somewhat overestimating the

added mass. The drag coefficient is modelled well, with better agreement of the results for higher KC (FIGURE 13).

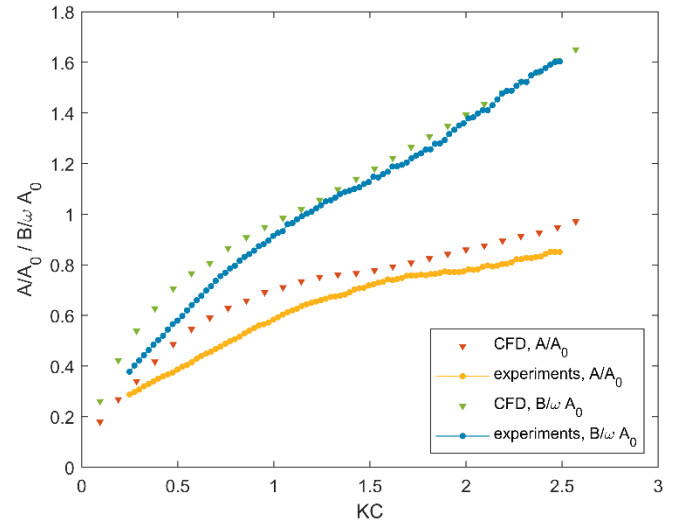


FIGURE 13 Added mass of the module without any contents (PP&4P43B), $H = 0.12\text{m}$; $T = 2\text{s}$. Comparison of CFD and experimental results.

4.4. Estimation of coefficients by summation

This Section discusses the estimation of hydrodynamic coefficients for the complete structures by summation of the coefficients for the individual components – schematically presented in FIGURE 14. The results are shown for the model consisting of the perforated plate, the mudmat and the staggered grid of 35 slender cylinders (PP&4P43B&35SQ), as seen in FIGURE 15 and FIGURE 16.

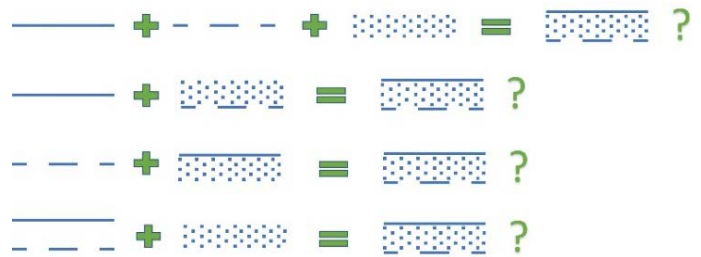


FIGURE 14 Schematic representation of summation of individual components and combinations in simplified subsea modules.

Summation was performed for each of the components tested alone (PP + 4P43B + 35SQ), as well as for the modules consisting of combinations of components summarized with a stand-alone element (PP + 4P43B&35SQ; PP&35SQ + 4P43B; PP&4P43B + 35SQ). Summation of the added mass for each of the components (PP + 4P43B + 35SQ) underestimates added mass for all tested KC. Other combinations are presented in FIGURE 15. The damping is overestimated by summation of any combination of the components (FIGURE 16). Combination of

the roof and the mudmat, added to the contents measured alone, provides the best estimation, with smallest discrepancy at small KC. In any case, the interaction between the elements increases the added mass and decreases the damping. These effects are not captured when the hydrodynamic coefficients are estimated by summation of stand-alone elements, leading to underestimation of the added mass and overestimation of damping. Summation of the coefficients for combined elements (4P43B&35SQ or PP&35SQ) with one stand-alone element, yields better results.

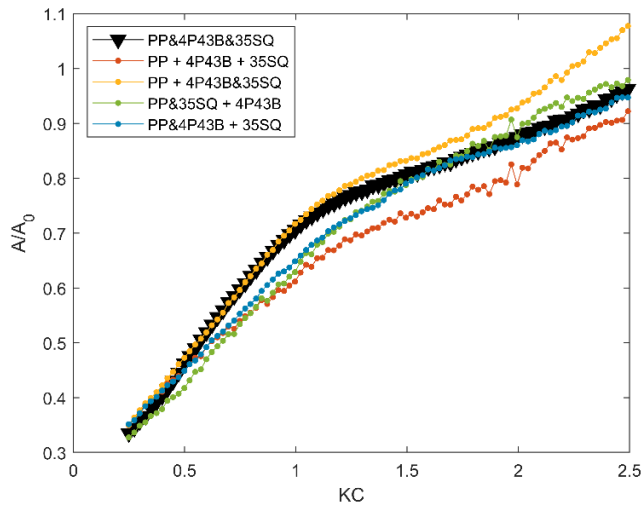


FIGURE 15 Experimentally estimated added mass for the simplified subsea module PP&4P43B&35SQ compared to the sum of added mass for various combinations of components. $H = 0.12\text{m}$; $T = 2\text{s}$.

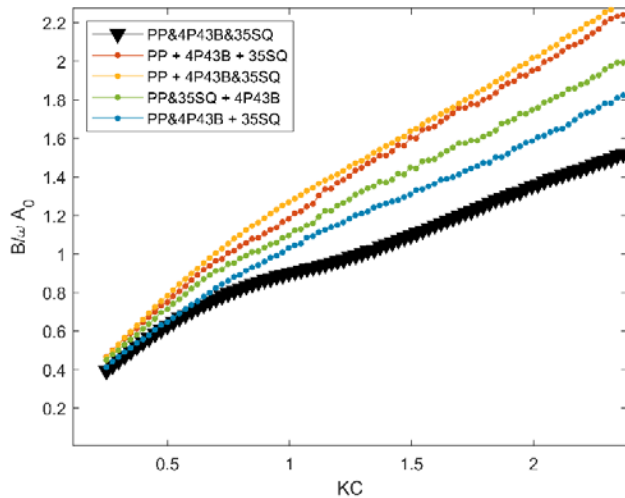


FIGURE 16 Experimentally estimated damping for the simplified subsea module PP&4P43B&35SQ compared to sum of damping for various combinations of components. $H = 0.12\text{m}$; $T = 2\text{s}$.

Simplified modules consisting only of the roof and contents or mudmat and contents are schematically presented in FIGURE 17. For the model consisting of the mudmat and the contents, estimation by summation underestimates the added

mass and gives a good estimation of the damping (FIGURE 18, FIGURE 19). In case of the model combining the protection roof and the contents, estimation by summation overestimates the added mass for KC numbers less than 0.8 and underestimates it for larger KC numbers. The damping is completely dominated by the perforated plate and is overestimated if estimated by summation.



FIGURE 17 Schematic representation of summation of individual components in modules with only roof/mudmat and contents.

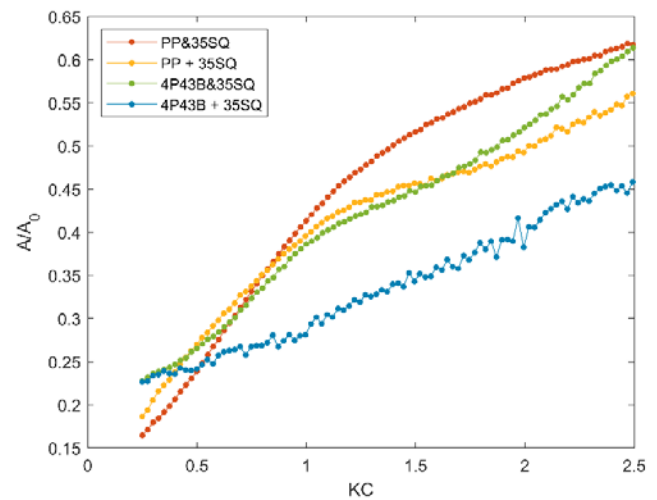


FIGURE 18 Experimentally estimated added mass for simplified subsea modules (PP&35SQ and 4P43B&35SQ) compared to the sum of added mass for the combinations of components. $H = 0.12\text{m}$; $T = 2\text{s}$.

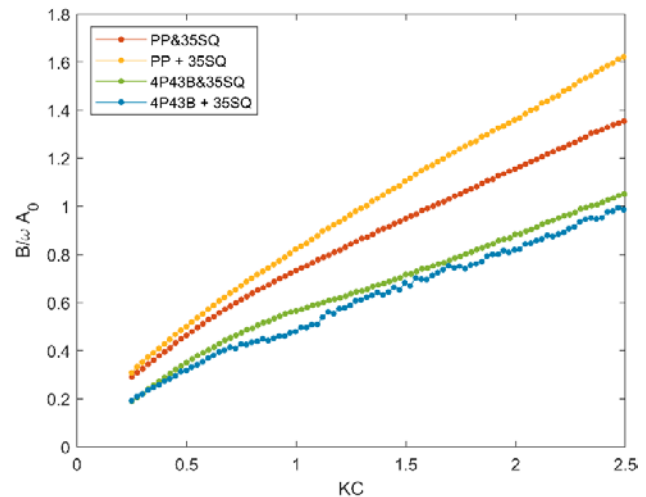


FIGURE 19 Experimentally estimated damping for simplified subsea modules (PP&35SQ and 4P43B&35SQ) compared to the sum of damping for the combinations of components. $H = 0.12\text{m}$; $T = 2\text{s}$.

5. CONCLUSIONS

Hydrodynamic coefficients for the simplified subsea modules and their components are studied experimentally by use of forced oscillation tests for fully submerged, nearly two-dimensional generalized models. The main conclusions are:

- For the tested modules, damping is generally the dominating hydrodynamic force. The presence of contents inside the modules will generally increase the importance of added mass compared to a module consisting only of a mudmat and a protection roof.
- The largest added mass is observed for the module with content consisting of five large squares. On the other hand, the presence of contents is reducing the damping. Still, the damping force is generally dominant.
- The content consisting of a single square has little influence on the coefficients, compared with the same module without any content.
- The volume of the single square and the content consisting of a staggered grid with 35 rectangular cylinders is nearly equal. Still, added mass for the module with the staggered grid is between 15 and 30 percent larger. The difference in damping is small.
- Added mass for the module consisting of the perforated plate (protection roof) and the staggered grid are fairly similar to the added mass of the module consisting of the mudmat and the staggered grid. On the other hand, the damping is 30 to 50 percent higher. This shows that the perforated plate used to model the roof, is of great importance for the damping. The perforated plate gives the major contribution to damping - the damping of the perforated plate alone and the model consisting of plate and staggered grid is nearly identical.

Estimation of hydrodynamic coefficients by summation of the coefficients for the individual structure members:

- The damping is generally overestimated when estimated by summation of the damping for the individual structure elements, compared to the tests of the entire modules.
- Considering added mass, estimation based on summation gives generally good results for the structures consisting of a mudmat and protection roof, with and without internal content. For the structures without a roof or a mudmat, the added mass estimated by summation is underestimated.

ACKNOWLEDGEMENTS

This work is performed as a collaboration between the Norwegian University of Science and Technology (NTNU) in Trondheim and SINTEF Ocean, financed by the Research Council of Norway, NFR project 237929 SFI/CRI Marine Operations MOVE, 2015 - 2023. We are grateful for the support and cooperation. The authors would also like to thank dr. Fredrik Mentzoni for sharing his expertise in numerical modelling.

REFERENCES

- [1] Sarpkaya, T., and Isaacson, M., 1981. *Mechanics of Wave Forces on Offshore Structures*. Van Nostrand Reinhold Co. Inc., New York.
- [2] Sumer, B. M., and Fredsøe, J., 1997. *Hydrodynamics Around Cylindrical Structures*. Advanced Series on Ocean Engineering—Vol. 12, World Scientific Publishing Co. Pte. Ltd., Singapore.
- [3] DNVGL AS. Recommended Practice, 2017. *Modelling and Analysis of Marine Operations*. DNVGL-RP-N103.
- [4] Molin, B., 2011. Hydrodynamic modelling of perforated structures. *Applied Ocean Research*, 33(1), pp. 1-11.
- [5] An, S. and Faltinsen, O. M., 2013. An experimental and numerical study of heave added mass and damping of horizontally submerged and perforated rectangular plates. *Journal of Fluids and Structures*, 39, pp. 87-101.
- [6] Tian, X., Tao, L., Li, X., and Yang, J., 2017. Hydrodynamic Coefficients of Oscillating Flat Plates at $0.15 < KC < 3.15$. *J.Mar. Sci. Technol*, 22(1), pp. 101–113.
- [7] Sarkar, A., Gudmestad, O. T., 2010. Splash Zone Lifting Analysis of Subsea Structures. OMAE2010-20489, pp. 303-312.
- [8] Mentzoni, F., Kristiansen, T., 2019. Numerical modeling of perforated plates in oscillating flow. *Applied Ocean Research*. vol. 84.
- [9] Mentzoni, F., Kristiansen, T., 2019. A Semi-Analytical Method for Calculating the Hydrodynamic Force on Perforated Plates in Oscillating Flow. OMAE2019-95093. Volume 7A, pp. 1-11.
- [10] Mentzoni, F., Kristiansen, T., 2020. Two-dimensional experimental and numerical investigations of perforated plates in oscillating flow, orbital flow and incident waves. *Applied Ocean Research*. vol. 97.
- [11] Solaas, F., Mentzoni, F., Abrahamsen-Prsic, M., Kristiansen, T., 2020. An Experimental and Numerical Study of Added Mass and Damping for Side-by-Side Plates in Oscillating Flow. *Journal of Offshore Mechanics and Arctic Engineering*, Vol. 143, 011901, pp. 1-12.
- [12] Mentzoni, F., Abrahamsen-Prsic, M., and Kristiansen, T., 2018. Hydrodynamic Coefficients of Simplified Subsea Structures. OMAE2018-78315, pp. 1–11.
- [13] Faltinsen, O. M., 1993. *Sea Loads on Ships and Offshore Structures*. Cambridge Ocean Technology Series. Cambridge University Press.
- [14] Solaas, F., Mentzoni, F., Abrahamsen-Prsic, M., Kristiansen, T., 2019. An Experimental and Numerical Study of Added Mass and Damping for Side-by-Side Plates in Oscillating Flow. OMAE2019-96008, pp. 1-10.
- [15] Mentzoni, F., 2020. *Hydrodynamic Loads on Complex Structures in the Wave Zone*. Doctoral thesis at NTNU, Trondheim, Norway. 2020:159, ISBN 978-82-326-4666-1.